Journal of Environmental Chemical Engineering 14 (2026) 123660

Contents lists available at ScienceDirect

Journal of Environmental Chemical Engineering

journal homepage: www.elsevier.com/locate/jece

Kinetic study of microplastic reactivity with hydroxyl radicals: Insights into photochemical fate and transformation products

Ádila O.S. Dantas [a,*], José Luis Fonseca [b], Raghav Dogra [b], Monica Passananti [b,c], Francesco Calore [d], Elena Badetti [d], Antonio Marcomini [d], Geovânia C. Assis [a], Luca Carena [b], Antonio C.S.C. Teixeira [a], Davide Vione [b,*]

[a] AdOx – Research Group in Advanced Oxidation Processes, Department of Chemical Engineering, Escola Politécnica, University of São Paulo, São Paulo 05088000, Brazil
[b] Dipartimento di Chimica, Università di Torino, Via Pietro Giuria 5, Torino 10125, Italy
[c] Institute for Atmospheric and Earth System Research, University of Helsinki, Helsinki 00014, Finland
[d] Department of Environmental Sciences, Informatics and Statistics, Ca' Foscari University of Venice, Via Torino 155, Venice 30172, Italy

ARTICLE INFO

Keywords:
Polymer photodegradation
Photolysis
Microplastic aging
Degradation pathways

ABSTRACT

Plastic pollution in the form of microplastics (MPs) poses a significant environmental threat, due to the widespread dispersion and persistence of these materials in aquatic ecosystems. This study investigates the reactivity of polyethylene (PE), polypropylene (PP), and polyvinyl chloride (PVC) MPs with hydroxyl radicals ($HO^{\bullet}$) through a kinetic competition method, using sodium benzoate (NaBz) as a reference compound with selective $HO^{\bullet}$ reactivity. Photosensitization by $NaNO_3$ under UV-B irradiation was employed as known $HO^{\bullet}$ source. The first-order reactivity constants for PE and PP MPs were ($\mu \pm \sigma$) $k_{PE} = (6.58 \pm 4.99) \times 10^4\ s^{-1}$ and $k_{PP} = (6.24 \pm 2.98) \times 10^4\ s^{-1}$, respectively. On the other hand, the reactivity of PVC MPs was influenced by reactions with organic compounds leached from the plastic material. Long-term photodegradation experiments revealed some small morphological changes in PE and PP MPs as a result of photoaging. The process also produced low molecular weight organic compounds, including short-chain carboxylic acids, and indicates that the presence of anions such as acetate and (in the case of PVC) chloride is associated with the photodegradation processes of the investigated MPs. FTIR spectroscopy suggested the presence of carbonyl groups, associated with oxidation of the polymer chains and the possible presence of plastic additives. Transformation products (TPs) were elucidated, indicating dechlorination processes for PVC MPs and/or the organic compounds they carried, and hydrogen abstraction, primary oxidation, dehydrogenation, and oxidative cleavage for PE and PP MPs.

1. Introduction

Plastic pollution is one of the most important environmental challenges of our time, due to the vast amount of improperly discarded plastic waste that pollutes oceans, rivers, soil, and even the atmosphere [1,2]. Among the most concerning aspects of this pollution are microplastics (MPs), i.e., plastic particles less than 5 mm in diameter, and nanoplastics (NPs), which are even smaller, measuring less than 1 μm [3]. MPs and NPs can be intentionally manufactured on a micro- or nano-scale (primary micro- and nanoparticles), or they can originate from the degradation of larger plastics, such as synthetic fabrics and football pitches (secondary micro- and nanoparticles) [4]. Polyethylene (PE), polypropylene (PP), polystyrene (PS), and polyvinyl chloride (PVC) are some of the most commonly used plastic materials [5,6].

Once in surface waters, MPs may be subject to mechanical abrasion caused by water flow dynamics and to hydrolysis, as well as to biodegradation and photodegradation processes [7]. Due to the high availability of solar energy in surface waters, photodegradation represents a key mechanism driving the breakdown of many micropollutants. MPs may degrade through direct photolysis, which involves mechanisms such as fragmentation, rearrangement, hydrogen and electron transfer [8,9], or via indirect photochemistry, mediated by attacks from photoproduced reactive intermediates (PPRIs), including hydroxyl radicals ($HO^{\bullet}$), singlet oxygen ($^1O_2$), triplet excited states of chromophoric dissolved organic matter ($^3CDOM^*$), and the carbonate radical anion ($CO_3^{\bullet-}$) [10]. Due to their rapid consumption in surface waters, PPRIs

* Corresponding authors.
E-mail addresses: adila.dantas@usp.br (Á.O.S. Dantas), davide.vione@unito.it (D. Vione).

https://doi.org/10.1016/j.jece.2026.123660
Received 11 March 2026; Received in revised form 9 June 2026; Accepted 15 June 2026
Available online 17 June 2026

occur at low steady-state concentrations, which typically range between 10^{-17} and 10^{-15} mol L^{-1} [11]. These reactive species are generated by the absorption of solar energy by photosensitizing compounds such as nitrate (NO_3^-), nitrite (NO_2^-), and chromophoric dissolved organic matter (CDOM) [12]. Among PPRIs, the hydroxyl radical is the most reactive species in natural waters ($E_0 = 2.80$ V vs SHE) and it is primarily produced through the photolysis of nitrate (NO_3^-) and nitrite (NO_2^-) ions. Nitrate exhibits a peak absorption in the UV-B region, with a maximum at 305 nm, while nitrite also absorbs UV-A sunlight [5]. Moreover, CDOM is an important $HO^\bullet$ source in organic-rich waters [9].

Plastics contain various substances that are not chemically bound to the polymer matrix, including unreacted monomer units, chemical additives such as antioxidants, plasticizers, and flame retardants, as well as processing aids such as catalysts, solvents, and lubricants [13]. The photodegradation of polymeric particles in the environment can lead to changes in the physicochemical properties of materials and the release of plastic additives and byproducts [14]. Depolymerization is one of the main degradation mechanisms, involving the cleavage of polymer chains that occurs more frequently at chain ends. Conversely, chain scission occurs when atoms or side groups attached to the polymer backbone are released [15]. Chromophoric functional groups and unsaturated bonds accelerate photodegradation, and conjugated double bonds additionally exhibit lower bond strength that allows them to be readily broken into smaller fragments [7].

Photodegradation represents the most significant pathway for abiotic oxidation in MP degradation [16,17], an oxidative process that occurs naturally in surface waters. Most published studies aim to investigate the harmful effects of rampant MP pollution or detect the presence of MPs in various environmental compartments. However, there is still a scarcity of research focused on evaluating the degradation kinetics and mechanisms of these materials, which could contribute to understanding the environmental fate of MPs through photoinitiated reactions. Furthermore, there is a lack of knowledge concerning the reactivity of the polymer backbone vs. additives and other compounds, which could all be involved in the scavenging of PPRIs such as $HO^\bullet$.

To address this gap, the present study aimed to investigate the reaction kinetics and pathways of MPs with hydroxyl radicals ($HO^\bullet$), using a kinetic competition approach that allows for the determination of reaction rate constants. Three MPs that would derive from materials widely used in plastic packaging, i.e., PVC, PP, and PE, were selected. They range from simple aliphatic polymers to structures with functional groups directly attached to the polymer backbone, which enables the comparison of variations associated with the polymeric structure. The experimental procedures were also devised to distinguish between the reactivity of the polymer itself and that of loosely bound compounds such as the additives. In addition, long-term photochemical experiments allowed for the identification of transformation products, derived from the oxidative photo dissolution of MPs. The study further assessed material aging indicators, offering valuable insights into the environmental degradation mechanisms of MPs.

2. Materials and methods

2.1. Chemicals

Sodium benzoate (≥ 99.0%, Sigma-Aldrich) was used as the reference compound to measure reaction rate constants with $HO^\bullet$, while sodium nitrate (≥ 99.0%, Sigma-Aldrich) was used to generate $HO^\bullet$ radicals. Polyvinyl chloride (PVC, GuanBu-Tech, Shanghai, China), polypropylene (PP, generated by cryogenic grinding of PP fragments) and polyethylene (PE, Cospheric, CA, USA) were used as model MPs for $HO^\bullet$ reactivity studies. For analysis (elution) with HPLC-DAD (high-performance liquid chromatography interfaced with diode-array detection), methanol and phosphoric acid (H_3PO_4, 85%) were purchased from Sigma-Aldrich. All solutions were prepared using ultrapure water with a resistivity of 18.2 MΩ cm and TOC < 3 ppb, obtained from a Milli-Q® system.

2.2. Kinetic competition experiments

The experimental conditions were designed to balance environmental relevance and experimental control. The potential aggregation of MP particles can influence their dispersion in the medium and affect photochemical processes. In the present study, experimental strategies were employed to minimize particle aggregation. MP suspensions were prepared with 16.5 mg of plastic powder in 100 mL of ultrapure water. The suspensions were first ultrasonicated for 4 min to promote disaggregation, and then magnetically stirred for 3 h at 80 rpm. Due to the intrinsic hydrophobicity of MPs, the dispersions were manually stirred vertically every hour to further maintain homogeneity. The MPs load used was higher than that typically found in surface waters. This approach was intended to ensure the applicability of the kinetic competition method and to minimize uncertainties associated with the heterogeneity of the system. Additionally, the MP load was kept constant in all kinetic experiments, to consider possible light scattering effects.

A kinetic competition method, well described by Zhou and Mopper [18], was used to predict the reactivity of the selected MPs with $HO^\bullet$. Sodium benzoate (NaBz) was employed as the reference compound with known $HO^\bullet$ reactivity and its initial concentration was varied in different experiments (2.5, 5.0, 15, 40, and 70 μmol L^{-1}), while the MP loading was always kept at 165 mg L^{-1}. In this way, the possible scattering of radiation by the MPs would be the same in all the irradiation experiments and would not affect significantly the measurement of the reaction rate constant between MPs and $HO^\bullet$. Furthermore, the use of a relatively high MP load was required by the need to scavenge $HO^\bullet$ significantly in comparison with the benzoate reference, thereby allowing for a proper kinetic competition between MPs and the reference compound. The use of lower MP loads would cause insignificant scavenging of $HO^\bullet$ and prevent a proper measurement of the reaction rate constant between MPs and $HO^\bullet$. For similar reasons, the initial NaBz concentration was varied in a range that enables quantification by liquid chromatography and encompasses conditions where benzoate is either a minor or the main $HO^\bullet$ scavenger in the system.

Hydroxyl radicals were generated photochemically from sodium nitrate ($NaNO_3$, 10 mmol L^{-1}) and their steady-state concentration was estimated by the pseudo-first-order degradation rate constant of sodium benzoate, using its known second-order rate constant with $HO^\bullet$ ($k_{Bz-,HO^\bullet} = 5.9 \times 10^9$ L mol^{-1} s^{-1}; [19]). The result was $[HO^\bullet]_{ss} = 10^{-14}$–$10^{-15}$ mol L^{-1}. This is in the upper range of the typical steady-state $[HO^\bullet]_{ss}$ values in surface waters (Vione et al., 2014). Nitrate was selected as $HO^\bullet$ source because it is an environmentally relevant photosensitizer compound in surface waters, in which NO_3^- ions absorb solar radiation in the UV-B region and generate $HO^\bullet$ [19]. Note that MPs can act as both scavengers and sources of $HO^\bullet$ radicals under irradiation [20]; however, regardless of how MPs affect the $HO^\bullet$ balance, the overall effect is accounted for in $[HO^\bullet]_{ss}$. Moreover, the kinetic model (see Section 6 in the Supplementary Material) considers the total formation rate of $HO^\bullet$, regardless if these are produced by nitrate alone or by additional sources as well.

The aliquots of the suspensions to be irradiated (total volume of 15 mL each) were placed in four cylindrical Pyrex glass cells (2.4 cm in height, 4.0 cm in diameter, cut-off wavelength of 280 nm). These cells have a side neck for inserting and removing liquids, which was securely sealed with a screw cap and kept in the same position during all irradiation experiments, which lasted for up to 2 h. The experiments were conducted under magnetic stirring at 80 rpm; irradiation was provided by a UV-B lamp (Philips TL 20 W/01) with maximum emission at 313 nm, a wavelength that corresponds to the most effective spectral range for NO_3^- absorption. Thus, the choice of a specific wavelength aims to reproduce the portion of the solar spectrum that is mainly responsible for triggering photochemical reactions by nitrate in surface waters. The

irradiance was 4.0 ± 0.2 W m^{-2} in the 300–400 nm range and T = 21.0 ± 3.0 °C. Samples withdrawn over a period of 2 h were filtered through 0.22 μm nylon membranes (Sartorius®), and NaBz concentrations were quantified by HPLC-DAD (see Section 4.1, Supplementary Material).

The kinetic competition experiments were carried out in the presence of MPs in ultrapure water and with the wash water from the MPs. The latter experiments were carried out to investigate the potential reactivity of the $HO^{\bullet}$ radical with compounds leached from MPs, which could interfere with the measurement of the $HO^{\bullet}$ reactivity attributed to the polymer backbone. To prepare the MPs wash water, 16.5 mg of MPs were suspended in 100 mL of ultrapure water and subjected to ultrasound pre-treatment for four minutes, followed by stirring at 80 rpm for three hours under identical conditions to those used in the kinetic competition experiments in the presence of MPs. The resulting suspension was then filtered via vacuum filtration using a cellulose acetate membrane (0.22 μm pore size). The filtrate, referred to as wash water, contains only the compounds released from the MPs. This wash water was subsequently used to evaluate potential interactions of these compounds with $HO^{\bullet}$ radicals.

The same experimental setup used in the kinetic competition experiments was employed to conduct long-term photochemical experiments (14 days) to promote the aging of MPs (see Section 3, Supplementary Material). At the end of the exposure, aliquots were collected and filtered (0.22 μm nylon filters) for total organic carbon (TOC) analysis, anions analysis by ion chromatography (IC), and identification of by-products by liquid chromatography – high resolution mass spectrometry (LC-HRMS); all analytical methods are described in Section 4 of the Supplementary Material. In addition, the liquid phase was vacuum-filtered using a cellulose acetate membrane (0.22 μm) and the MPs were recovered and dried at room temperature, for characterization by scanning electron microscopy (SEM) and by attenuated total reflectance – Fourier transform infrared spectroscopy (ATR-FTIR), to assess potential signs of aging of the material surface.

The competition model used does not explicitly account for effects associated with particle heterogeneity or light scattering in systems containing MPs. However, to evaluate possible light scattering effects caused by MPs in the system, experiments were performed using 2-nitrobenzaldehyde (2-NB), based on the methodology described by Allen et al. [21]. The experiments were carried out under UV-B irradiation, comparing two conditions: (i) 2-NB solution (100 μmol L^{-1}) in the absence of MPs and (ii) 2-NB solution in the presence of MPs (0.165 g L^{-1}). The degradation of 2-NB was monitored by HPLC and described by pseudo-first order kinetics, allowing the reaction constants (k) to be determined. The comparison between the values of k obtained in the absence and presence of MPs was used as an indirect metric of photon availability in the system, expressed by an attenuation factor (k_{ii}/k_i), where k_i is the pseudo-first order kinetic constant of 2-NB in the absence of MPs and k_{ii} refers to the kinetic constant obtained for 2-NB in the presence of MPs.

2.3. Characterization of microplastics

The morphology of PVC, PP, and PE was analyzed using SEM with an electron gun (FEG Schottky). Secondary electron images were obtained using a FEI microscope (Inspect F50) operating at 5 kV. The particle size of microplastics (MPs) was assessed by examining scanning electron microscopy (SEM) images utilizing ImageJ software. A randomly selected subset of particles served as the basis for analysis, with equivalent diameter employed as the standard metric for size determination. All MPs had a particle size in the range of 1.0–4.0 μm (Table S1).

To characterize the functional groups on the surface of the MPs, ATR-FTIR analysis was performed using a Fourier transform infrared spectrometer (Alpha II, Bruker®) from 4000 to 400 cm^{-1} for 64 scans, with a resolution of 4 cm^{-1}. For each sample, 2–3 replicates were collected. The spectral data was processed using Omnic® 8.0 and Origin® 8.0 software.

The chemical state of the surface of the pristine MPs was analyzed through X-ray photoelectron spectroscopy (XPS) using a conventional XPS spectrometer (ScientaOmicron ESCA+) with a high-performance hemispheric analyzer (EAC2000) with 128 channels and with monochromatic Al Kα ($h\nu = 1486.6$ eV) radiation as the excitation source. The operating pressure in the ultra-high vacuum (UHV) chamber during analysis was 10^{-9} Pa. The XPS high-resolution spectra were recorded at a constant pass energy of 30 eV with a step size of 0.05 eV. An electron flood gun (CN10) was used as a standard charge neutralizer. The binding energies were measured in reference to the C 1 s peak at 284.8 eV. The XPS spectra were analyzed using CASA_XPS software.

3. Results and discussion

3.1. Reactivity of MPs with $HO^{\bullet}$ radicals

In the first place, regarding the possible scattering caused by the incidence of light on the MPs, the results of the attenuation factor (Table S2) were evaluated. No significant differences were observed between the conditions applied for the different MPs (PE, PP, and PVC) and the test conducted in the absence of MPs. Therefore, there is no significant evidence of attenuation of incident radiation associated with light scattering by the MPs in this case. These results suggest that optical effects, such as scattering, do not play a dominant role when MPs are added to the system. In any case, a constant MP load was used throughout the experiments to minimize the effect of light scattering.

For each MP, photochemical experiments were performed with different initial concentrations of the reference compound (NaBz) and maintaining the MP loading constant, as mentioned before [22]. For each initial concentration of Bz^-, the pseudo-first-order kinetic constants of the reference compound (k_{Bz^-}) were obtained from the slope of the $-\ln [Bz^-]/[Bz^-]_0$ *vs.* time graphs. Next, the degradation rates (R_{Bz^-}) (Table S3) were calculated from the product $k_{Bz^-} \times [Bz^-]_0$. The experimental results of the Bz^- degradation rate profiles in the presence of $Bz^- + NO_3^-$ and of PE, PP, or PVC are shown in Fig. 1, together with the fitting curves obtained using **Eq. (10)** in the Supplementary Material. Such an equation was derived from a kinetic model that took into account $HO^{\bullet}$ photogeneration by the irradiated solution ($R_{HO^{\bullet}}$) and the $HO^{\bullet}$ reaction kinetics with the polymer (k_{MPs}), with water-released compounds (wash water, k_{ww}), and with other solution components including nitrate (k_{sc}) (see Section 6 in the Supplementary Material). Note that k_{MPs} is the first-order reaction rate constant of $HO^{\bullet}$ and MPs, while k_{ww} refers to the wash water experiments (without MPs), and k_{sc} to the system in the absence of either wash water (ww) or MPs.

The trend of R_{Bz^-} *vs.* $[Bz^-]_0$ with only $Bz^- + NO_3^-$ (i.e., without MPs or ww) was fitted with **Eq. (10)**, with fixed $k_{MPs} = k_{ww} = 0$ and k_{sc} as the fitting variable, the value of which could thus be obtained. The same equation was used in the case of experiments with ww, keeping $k_{MPs} = 0$, $k_{sc} = (1.33 \pm 0.34) \times 10^4$ s^{-1} as per the previous fit, and with k_{ww} as the fitting variable. Finally, in the case of the experiments with MPs, **Eq. (10)** was used for data fitting with fixed values of k_{sc} and k_{ww} according to the previous calculations, and with k_{MPs} as the fitting variable.

Benzoate was chosen as the reference compound because, under nitrate irradiation, it reacts selectively with $HO^{\bullet}$ [23]. This selectivity primarily arises from the hydroxylation of the aromatic ring, as demonstrated by Zhou and Mopper [18], who showed that the reaction yields *ortho*-, *meta*-, and *para*-hydroxybenzoate isomers in characteristic proportions. According to the authors, this product distribution remained constant across diverse aqueous matrices (seawater and freshwater) despite the presence of competing reactive species, confirming that the reaction is predominantly driven by $HO^{\bullet}$. Crucially, the authors validated this method using methanol as an independent second probe; despite entirely different reaction mechanisms, the convergence of results confirms that benzoate accurately monitors hydroxyl radical reactivity, establishing it as a highly specific probe. Thus, in the present work, since the formation of hydroxylated products is closely linked to

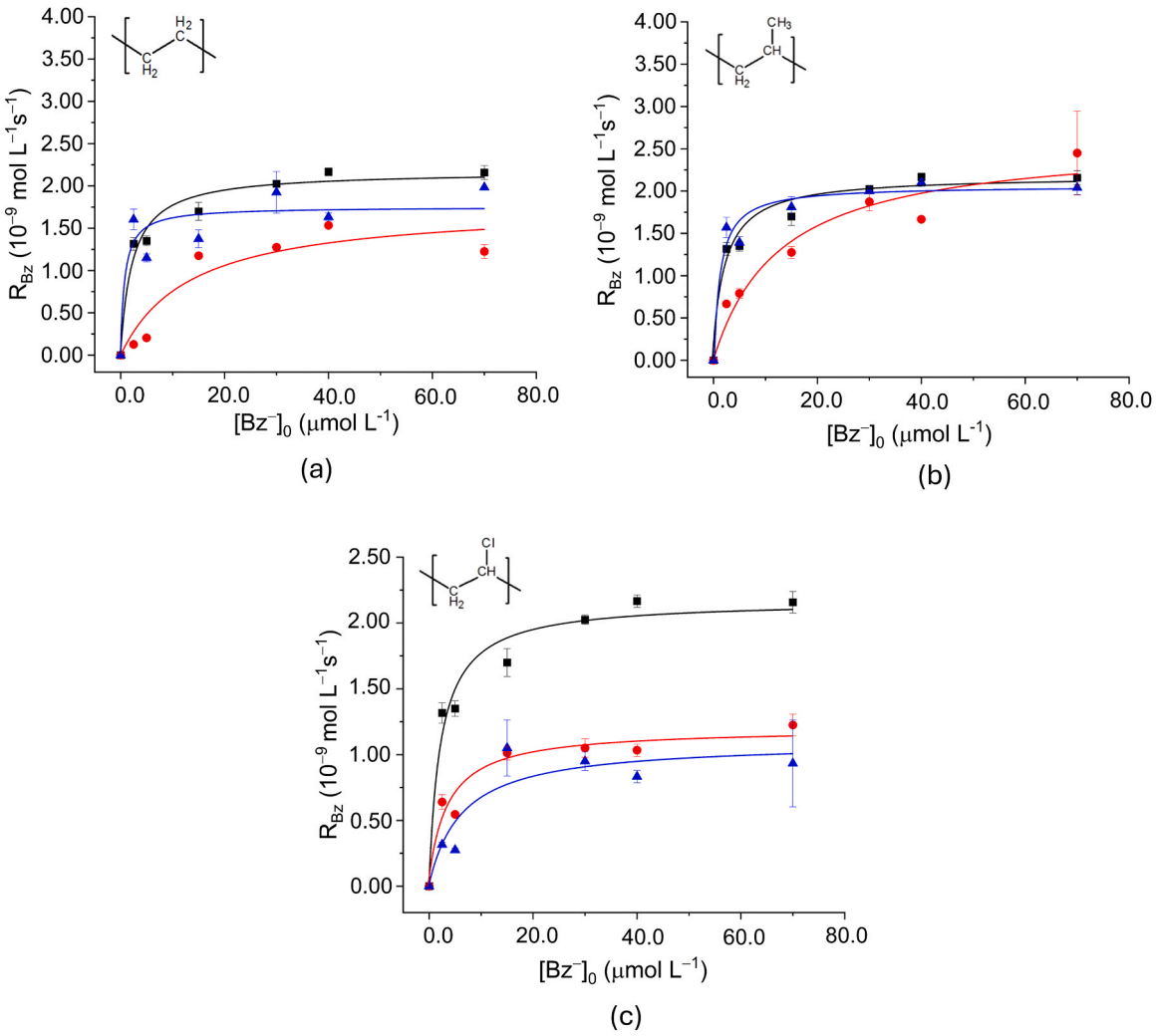

Fig. 1. Bz^- degradation rate profile (R_{Bz^-}) under UV-B irradiation, as a function of the initial concentration of Bz^- ($[Bz^-]_0$), with 10 mmol L^{-1} $NaNO_3$ alone (■), in the presence of 10 mmol L^{-1} $NaNO_3$ spiked to the wash water (▲), and in the presence of 10 mmol L^{-1} $NaNO_3$ + 165 mg L^{-1} MPs (●). **(a)** PE, **(b)** PP and **(c)** PVC.

$HO^•$, interference from reactive nitrogen species (RNS) generated during nitrate irradiation is minimized, ensuring that the calculated reaction rate constant reflects only $HO^•$-mediated pathways. Importantly, the selectivity of sodium benzoate (NaBz) for $HO^•$ does not imply that all observed transformations in microplastics (MPs) are caused exclusively by this radical. To delineate the individual contributions of other reactive oxygen species (ROS) or RNS, complementary experiments using selective scavengers alongside techniques such as electron paramagnetic resonance (EPR/ESR) spectroscopy combined with spin-trapping agents would be required to provide a more comprehensive mechanistic understanding.

Interestingly, for both PP and PE, $k_{ww} \sim 0$ were obtained, which means that the organic compounds released by the two polymers in aqueous solution would not contribute significantly to the overall scavenging of $HO^•$ in the systems under investigation. In contrast, there is evidence that both PE and PP significantly scavenge $HO^•$ radicals. If it is possible to exclude the role of released dissolved compounds, it is likely that the scavenging process is carried out by the polymer backbone. Considering that both PP and PE have saturated aliphatic chains on their surface, this finding is consistent with the fact that alkanes react readily with $HO^•$ [19]. Qualitatively, the ability of both PP and PE to scavenge $HO^•$ can be inferred by the fact that the relevant curves in Fig. 1 are clearly detached from the curves of experiments with nitrate alone and with the wash water. Quantitatively, from data fit, k_{MPs} values of $(6.58 \pm 4.99) \times 10^4$ s^{-1} for PE and $(6.24 \pm 2.98) \times 10^4$ s^{-1} for PP were obtained. Although PP and PE are both alkanes, they have different molecular structures. PP contains tertiary C–H bonds which are intrinsically more susceptible to hydrogen abstraction by $HO^•$ [24]. However, the presence of the lateral methyl group in PP can impose steric restrictions that limit the accessibility of radicals. In contrast, PE is composed of linear chains with accessible methylene groups, favoring exposure and radical attack. Also given the highly reactive and non-selective nature of $HO^•$, which tends to smooth structural differences as far as reactivity is concerned, these opposing effects likely offset each other, resulting in comparable apparent rate constants under the experimental conditions.

The results for PVC are shown in Fig. 1**(c)**. In this case, the scavenging of $HO^•$ by plastic is mostly accounted for by the compounds released in the solution ($k_{MPs} \sim k_{ww}$). In the case of PVC, it is possible that the polymer has chlorine atoms on its surface (see Fig. S1) that are likely little prone to $HO^•$ attack. In addition, compared to other plastics, PVC is one of the materials that uses the most additives in its production, especially plasticizers, 80% of which are used in PVC formulation [15, 25]. Therefore, it is likely that there is a release of organic compounds derived from plastic additives, which masks the reaction of the polymer itself with $HO^•$ radicals.

The interaction of PPRIs and their role in promoting the oxidation of polymer particle structures at the molecular level are not yet fully understood. Recent studies suggest that the photoaging process of NPs/MPs caused by PPRIs is primarily related to the cleavage of chemical

bonds and the subsequent formation of oxygen-containing functional groups [26]. The $HO^{\bullet}$ radical stands out as one of the main contributors to plastic photoaging. In sunlit waters, spectral intensity, depth of irradiation, and water chemistry vary significantly, which can result in formation rates of $HO^{\bullet}$ lower than those observed in the experiments with MPs. In addition, the presence of dissolved organic matter (DOM), bicarbonate, carbonate, and other compounds can scavenge $HO^{\bullet}$ [12]. Thus, the kinetic parameters obtained in this study should be interpreted as upper limits of the reactivity of MPs with $HO^{\bullet}$, as is the case for the estimated $[HO^{\bullet}]_{ss}$ values compared to typical levels found in sunlit natural waters, as observed previously. In aliphatic polymers such as PE and PP, the main mechanism of photoaging is through hydrogen abstraction, which is related to the stability of C—H bonds [14]. In addition to reactions with pure polymer matrices, the weathering process of MPs can release organic compounds into the environment, such as plastic additives including phthalates, bisphenols, and even organotin substances. Given that the hydroxyl radical is a highly reactive, non-selective species with a high oxidation potential ($E^0 = 2.8$ V SHE), it is known to trigger oxidation reactions with a variety of organic pollutants, including substances used as plastic additives [26,27]. For this reason, the organic compounds released by the three polymers under irradiation were identified.

Furthermore, it is worth noting the possible re-adsorption of these compounds onto the MPs surface, which can lead to the formation of an organic layer, changing properties such as polarity, hydrophobicity, and the availability of reactive sites. Such changes can affect the diffusion and interaction of $HO^{\bullet}$ radicals with the material surface. Furthermore, dissolved organic compounds can absorb UV radiation (the "inner filter" effect) or participate in secondary reactions, influencing the generation and fate of reactive species (see Fig. 4**(a)**) [28]. In the present study, these effects were partially accounted for through experiments with MP wash water, allowing for the evaluation of the contribution of leached species to the reaction system.

3.2. Impact of photodegradation on surface morphology

SEM analyses were performed to determine changes in the morphology and surface details of MPs during the aging process, due to photooxidation in the presence of $NaNO_3$ over two weeks. Fig. S2 shows micrographs of the MPs before and after treatment. Overall, the morphology differences observed were rather small. As can be seen in Fig. S2**(a)**, the PP particles before treatment had the shape of an irregular fragment with a rough surface. Aging (Fig. S2**(b)**) may have slightly increased the occurrence of fissures and cracks on the surface, which would also expose the pores inside the MPs as highlighted in the figure. Similarly, the PE MPs had an irregularly rounded shape and oriented wrinkles (Fig. S2**(c)**), which became more evident after aging (Fig. S2 **(d)**), suggesting that there might be a predominantly superficial oxidation process of the polymer. For PVC (Fig. S2**(e)** and Fig. S2**(f)**), two particle sizes can be identified, which are the result of the suspension polymerization process, where the primary particles aggregate into larger granules [29]. However, only a slight change in surface morphology could be observed after the aging process.

3.3. Microplastic chemical transformations resulting from photoaging

The quantification of the chloride, acetate and formate anions was carried out, along with the determination of the TOC concentration for the samples before and after photoaging, performed over two weeks (Fig. 2). The irradiation of nitrate would produce $HO^{\bullet}$ at a rate that can be assessed from the plateau reached by the degradation rate of benzoate at elevated Bz^- concentration, when Bz^- scavenges about the totality of photogenerated $HO^{\bullet}$. Indeed, from the kinetic competition model (see Section 6 in the Supplementary Material) it is derived that $\lim_{[Bz^-]\to\infty} R_{Bz^-} = R_{HO^{\bullet}}$. From Fig. 1, it can be inferred that the plateau reached by R_{Bz^-} at high $[Bz^-]$ is around 2×10^{-9} mol L^{-1} s^{-1}. Over a period of two weeks, such a rate might translate into a cumulative $HO^{\bullet}$ dose that could reach the mmol L^{-1} range as an order of magnitude.

Determining the ion concentrations before and after aging can provide insights into the degradation mechanisms of MPs. As shown in Fig. 2**(a)**, the PP MP suspension showed a significant increase in acetate (CH_3COO^-) concentration after irradiation (443.31 μmol L^{-1}), along with the detection of formate ($HCOO^-$) at low concentrations (23.68 μmol L^{-1}). In addition, a minimal presence of acetate was observed after irradiation of the PE MP suspension (8.93 μmol L^{-1}). These same anions were also detected by Bianco et al. [17], who evaluated the photodegradation of PS MP suspensions, showing a significant increase in concentrations after 90–100 h irradiation. There are reports in the literature that the photodegradation processes of MPs produce low molecular weight (LMW) acids, such as short-chain carboxylic acids (CH_3COOH and HCOOH) [14,30]. The presence of tertiary carbon and the subsequent branching with the methyl group ($–CH_3$) in the PP chain may facilitate the formation of acetate anions in the reaction medium [31]. In addition, LMW acids could derive from the transformation of polymer additives (*vide infra*). However, PVC MP suspensions showed

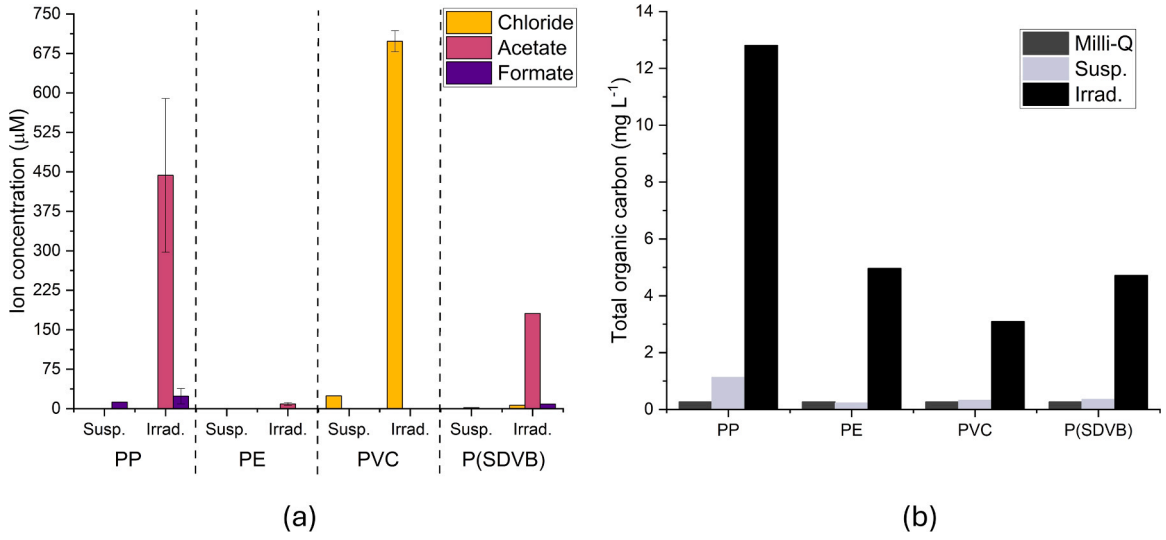

Fig. 2. (a) Ion concentrations and **(b)** TOC detected in MP suspensions (165 mg L^{-1}) before (Susp.) and after two weeks of irradiation in the presence of 10 mmol L^{-1} $NaNO_3$ + 165 mg L^{-1} MPs. The baseline TOC values in the ultrapure water used (Milli-Q) are also shown.

the presence of chloride anions, with high concentration after the aging process. This finding suggests that PVC MPs underwent a dechlorination process [26,32]. If dechlorination involved only or predominantly the smaller particles (see Fig. S2**(e)**), it is possible that the changes on the surface went unnoticed in the SEM micrographs. As an alternative, the release of chloride could take place upon transformation of polymer additives and/or incomplete polymerization leftovers.

Interestingly, the concentrations of acetate deriving from irradiated PP and of chloride from irradiated PVC, both in the sub-mmol L^{-1} range (Fig. 2**(a)**), are of the same order of magnitude as the cumulated $HO^{\bullet}$ dose produced by irradiated nitrate. This finding outlines the relationship between the aging process and the release of dissolved compounds by MPs.

When evaluating the variation in TOC concentration, Fig. 2**(b)**, of the MPs suspensions before and after aging, an increase in TOC was observed in all cases when compared to the respective suspensions before aging, suggesting that the rate of formation of organic products exceeded their rate of degradation, thereby allowing for TOC accumulation. In the case of PP, most of the TOC could be attributed to the formation of LMW acids, predominantly acetate and, in smaller amounts, formate, which together accounted for approximately 85% of the total TOC. In contrast, for PE, LMW acids contributed only about 4% of TOC, indicating that PE oxidation results mainly in more complex or partially oxidized organic products (*vide infra*).

Fig. 3 shows the FTIR spectra of (I) pristine MPs, (II) MPs after UV irradiation in the absence of $NaNO_3$, and (III) MPs after UV irradiation in the presence of $NaNO_3$ (photoaging involving $HO^{\bullet}$ in the latter case). As can be seen in Fig. 3**(a)**, the FTIR spectrum of pristine PP MPs shows typical bands in the range of 2838–2953 cm^{-1} related to asymmetric and symmetric stretching of CH_2 and CH_3 [33], and others at 1455–1375 cm^{-1} relating to CH_3 symmetrical bending [34]. The strong band at 1713 cm^{-1} and the shoulders at 1740 cm^{-1} and 1768 cm^{-1} are not attributable to the polymer structure of PP and may be associated with the carbonyl (C═O) vibration, possibly indicating the presence of one or more additives, which is consistent with the released TOC value shown in Fig. 2**(b)**. Upon irradiation, a decrease in the intensity of the band at 1713 cm^{-1} can be observed for both conditions II and III (Fig. 3**(b)**). Simultaneously, for condition III, a small new band appeared around 1630 cm^{-1}, which could be related to the oxidation of the polymer skeleton. In addition, it was possible to identify bands not attributed to PP between 1000 and 1200 cm^{-1}, which may be related to the presence of -CF and -CF_2 groups. Fluorinated bands may appear in PP and are related to surface modification performed to improve dye adhesion [35,36].

Fig. 3**(c)** shows the FTIR spectra of pristine PE MPs, and of irradiated PE MPs in the presence and absence of $NaNO_3$. The main FTIR bands related to pristine and aged PE MPs are located at 2914, 2847, 1472, 1462, 730, and 718 cm^{-1}, which were assigned to CH_2, C-H, and C-C vibrations [37,38]. As can be seen in Fig. 3**(d)**, a new signal at 1715 cm^{-1} appeared in the case of irradiated PE, and it was particularly high in the presence of $NaNO_3$. This band is associated with the vibration of the carbonyl group. According to the literature, the increase in signal intensity is related to the oxidative degradation that occurs during the weathering process under UV radiation and, more notably, exposure to $HO^{\bullet}$ radicals, reflecting the oxidation of the polymer skeleton [39]. At the same time, a decrease in signal intensity at 1560 cm^{-1} was observed. This band is not related to PE, but could be assigned to the presence of an additive containing amide groups, such as a hindered amine light stabilizer (HALS) [40], which is likely to be present at low concentration.

Regarding the FTIR analysis of PVC MPs, Fig. 3**(e)** shows the main bands identified at 2967, 2911, 1426, 1332–1253, 960, and 689–610 cm^{-1}, related to the C-H stretching neighboring C-Cl groups, C-H stretching, CH_2-Cl vibrations, C-H stretching or deformation, CH_2 rocking, and C-Cl stretching vibration, respectively [41–43]. When comparing the FTIR spectra of pristine and irradiated PVC MPs, no significant variations were observed. This indicates that aging did not lead to sufficient oxidation and did not cause major changes in the molecular structure of PVC, a result that is in line with the poor reactivity of the PVC skeleton towards the $HO^{\bullet}$ radical, as can be seen in Fig. 1**(c)**. A small band at 1735 cm^{-1}, related to C═O group vibrations, and some shoulders located at 1385 cm^{-1} and 758 cm^{-1} were not attributable to pristine PVC MPs. According to the literature, they can be associated with plasticizer additives, such as phthalates [44,45] or avobenzone (*vide infra*), indicating that the carbonyl signatures observed are predominantly derived from additives, rather than from oxidation processes of the PVC backbone.

The carbonyl index (CI), shown in Table S4, is a commonly used indicator of MP aging, particularly under photooxidative conditions. The CI is calculated as the ratio of the absorbance of the carbonyl (C═O) band, typically formed during oxidative degradation, to a reference peak corresponding to a stable functional group in the polymer matrix. The appearance of carbonyl groups is a hallmark of polymer oxidation, often resulting from exposure to UV radiation or reactions with oxidizing agents such as the $HO^{\bullet}$ radicals.

However, the presence of plastic additives containing oxygenated groups can interfere with this measurement, leading to misinterpretations about the actual state of degradation of the material. This effect can be observed in the CI values obtained for PP MPs, which showed a high initial value (CI = 2.137), even before artificial aging. This result suggests that pre-existing additives in the matrix may be responsible for the decrease in CI (0.467) during aging with nitrate, due to the degradation and leaching of carbonyl-containing additives. In contrast, PE MPs showed a low initial CI (0.036), with a slight increase after exposure to UV-B radiation (0.042) and, especially, in the presence of nitrate (0.083), evidencing the accumulation of carbonyl groups during photochemical aging. For PVC MPs, the initial CI was 0.121, which decreased to 0.080 in the presence of nitrate, although it was not possible to determine the value in the presence of UV-B alone. This behavior may indicate either a differentiated degradation of PVC, or analytical interferences associated with its structure or additive composition. In addition, both synchronous and asynchronous 2D-COS analyses may offer robust spectroscopic insight into the sequential evolution of functional groups during MP photoaging, thereby substantially strengthening the mechanistic elucidation of the underlying transformation pathways.

XPS analyses of the pristine MP samples revealed differences in surface chemical composition and in the functional groups present in each polymer. The survey spectra (Fig. S3) confirmed the predominance of characteristic C (1 s) signals at approximately 284.6 eV, as well as the presence of surface oxygen identified by the O (1 s) signal, in all MPs. For PP, an F (1 s) peak was also observed at 689.5 eV, while PVC exhibited characteristic Cl (2p) signals at 199.7 eV (Cl 2p3/2) and 201.3 eV (Cl 2p1/2), consistent with the chlorinated structure of the polymer. The high-resolution XPS spectra (Fig. S4) showed a predominance of C–C/C–H bonds for both PE and PP. However, both materials exhibited surface oxygenated groups, such as C–O, C–OH, and C═O, indicating a level of prior oxidation likely associated with industrial processing, storage, or the presence of additives incorporated into the polymer matrix. This behavior was even more evident in PP, which exhibited a greater diversity of oxygenated groups and higher surface chemical heterogeneity. In addition, PP presented signals attributed to fluorinated groups (–CF_2CF_2– and –CF_3), confirmed by the F (1 s) peak at 689.5 eV. The presence of these species may be related to surface fluorination treatments applied industrially to increase the wettability, adhesion, and affinity of the material for dyes and coatings [35,36].

3.4. Transformation products (TPs)

To better understand the types of products released into water following MPs degradation and to gain insight into potential transformation pathways, MP samples exposed to light and $NaNO_3$ for 14 days were analyzed using UHPLC coupled with a high-resolution mass

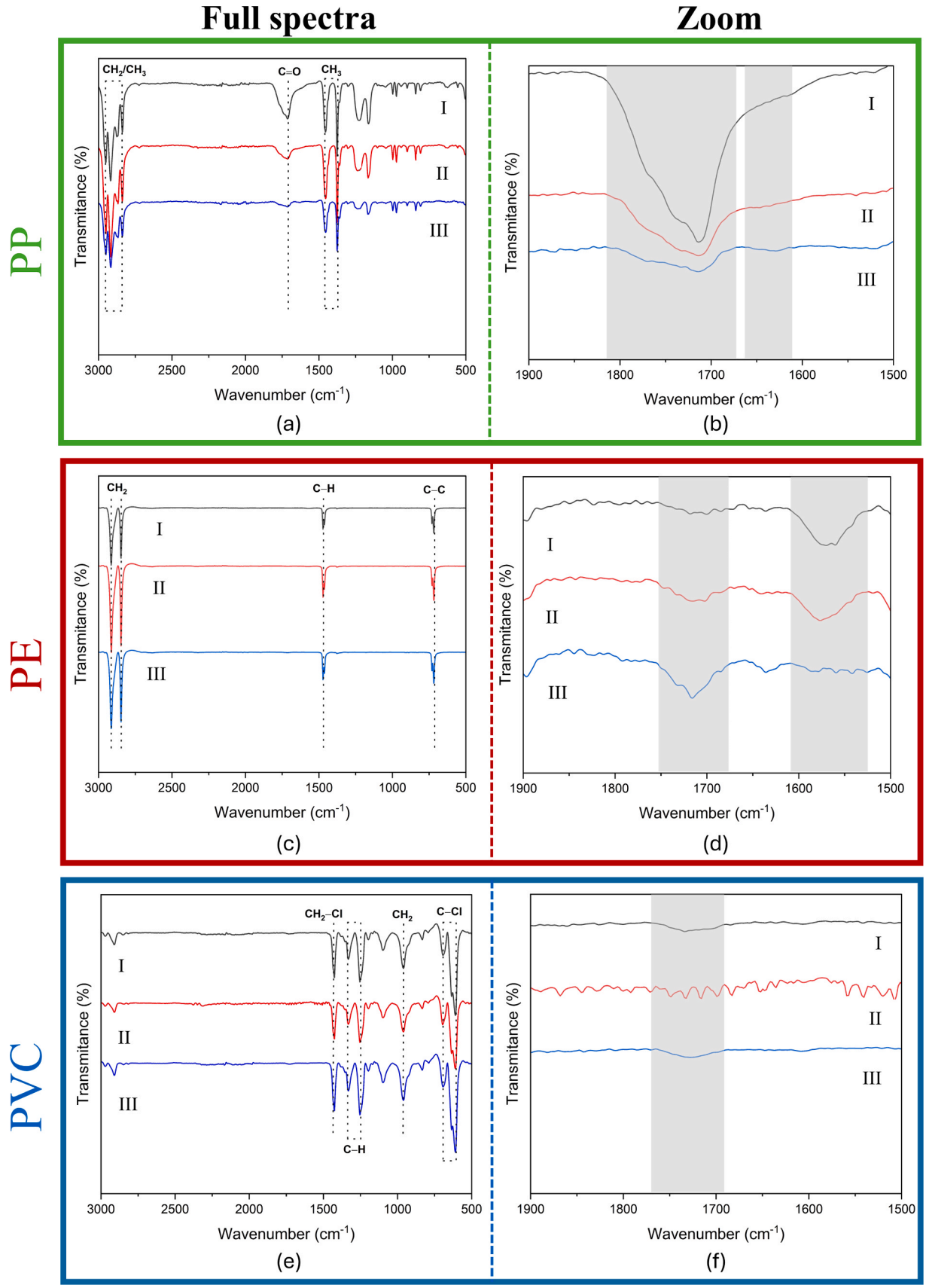

Fig. 3. FTIR spectra of PP MPs **(a,b)**, PE MPs **(c,d)**, and PVC MPs **(e,f)**. I= non-irradiated, II= irradiated in the absence of $NaNO_3$, and III= irradiated in the presence of 10 mmol L^{-1} $NaNO_3$.

spectrometer (Orbitrap HRMS). As control experiment, MP samples with $NaNO_3$ were kept in the dark for 14 days following the same analytical procedures to assess the leaching of additives and impurities not induced by light. The TPs reported in this study were detected exclusively in irradiated samples, after excluding common compounds to both irradiated and non-irradiated controls. This comparative approach indicates that the detected compounds arise as a consequence of photoirradiation rather than the direct release of pre-existing additives or impurities. Seventeen major TPs were identified, released into the aqueous phase. Ten TPs were identified for PVC, six for PE, and three for PP (two TPs were common to PVC and PE, see Table S5). The tentative structural identification was based on the retention behavior, accurate mass, isotopic pattern, and the interpretation of the MS^2 spectrum of the data-dependent tandem MS (ddMS) selected parent ion. Comparison with authentic reference standards was not possible, as these compounds are formed *in situ* and usually are not commercially available, which is a common limitation in studies dealing with environmental-like photo-oxidation, in particular with polymers and microplastic degradation. Accordingly, following the confidence levels described by Schymanski et al. [46], the proposed structures of the identified TPs should be regarded as tentative to probable. The LC-HRMS analysis was therefore intended to elucidate dominant transformation pathways and reaction classes rather than to provide unambiguous structural confirmation of individual compounds. In addition, structural isomers (e.g., hydroxylated products at different substitution sites) may form during photooxidative processes; their systematic discrimination was beyond the scope of this study. While the precise distinction between TPs originating from the polymer backbone and those derived from additive degradation cannot be unequivocally established (considering also that the type and amount of additives in plastics are often unknown), the observed

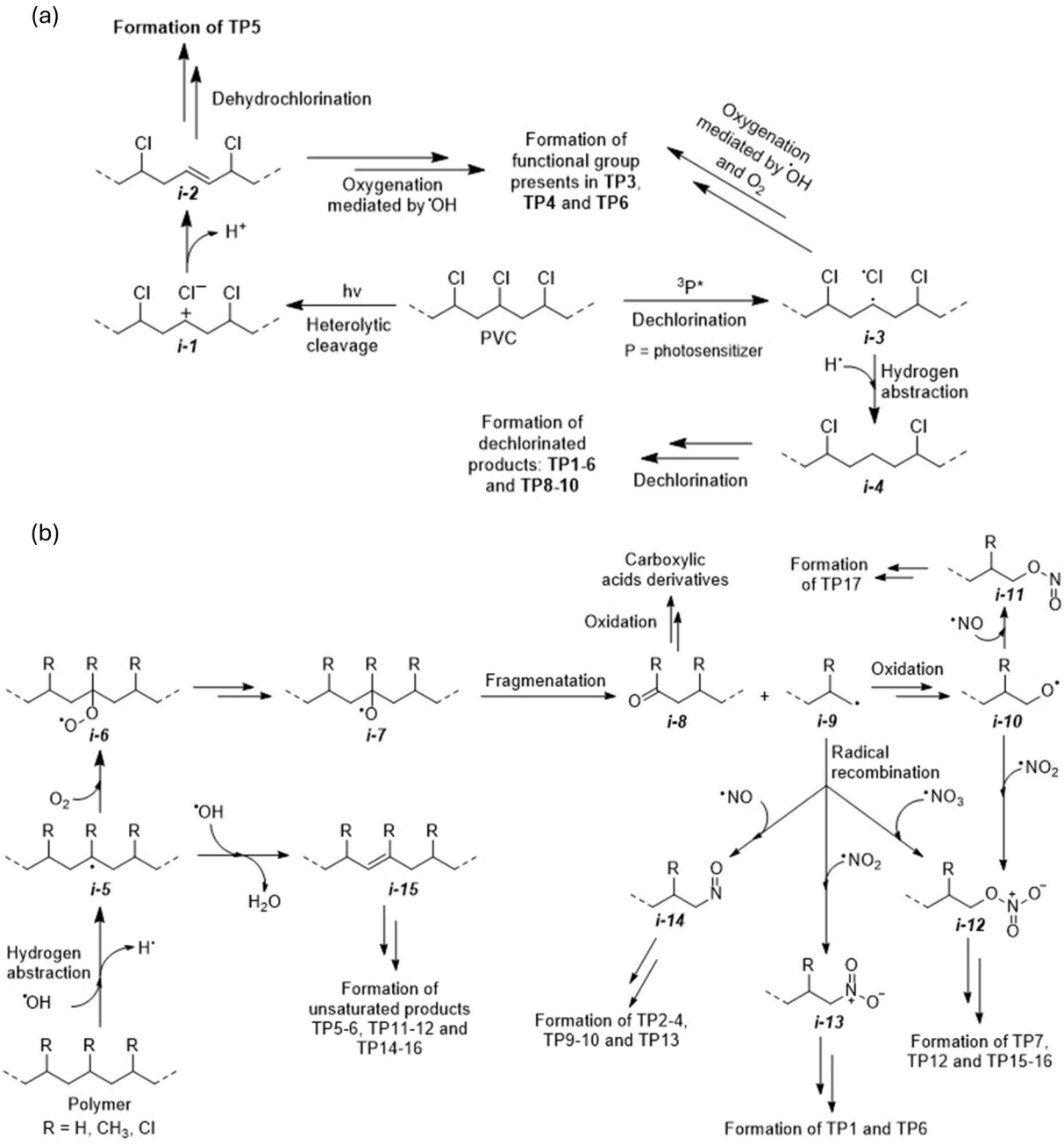

Fig. 4. (a) Possible simplified reaction pathways for (a) dechlorination of PVC MPs, after exposure to light and $NaNO_3$ over two weeks and (b) formation of *N*-derivatives and the unsaturated products, after exposure to light and $NaNO_3$ over two weeks.

irradiation-dependent formation confirms that these compounds are TPs generated during the photooxidative process. The identified TPs and their proposed structures are listed in Table S5.

Fig. S5 presents a schematic diagram illustrating the main TPs identified for PVC. The molecular complexity of these compounds suggests the occurrence of a series of reactions, such as dechlorination, dehydrochlorination, hydroxylation, nitrosation, oxidation, dehydrogenation, and chain scission, leading to several byproducts with distinct molecular weights [32,47]. In addition to photoinduced reactions, the differences between the identified TPs and the expected structure of the PVC polymer might also originate from structural irregularities in the polymer itself. During the polymerization process, chain transfer reactions involving the propagating radical formed from vinyl chloride can lead to the formation of various isomeric structures and structural defects [48]. Transformation of these defective sites would lead to TPs that differ from the parent polymer. Moreover, given the poor $HO^{\bullet}$ reactivity of the PVC skeleton, it is also likely that these compounds derive from additives or oligomerization leftovers that were not included in the polymer structure.

The most common TPs observed in this study with PVC had fewer chlorine atoms than expected from the PVC structure. This is evidenced by partial dechlorination in TP5 (673.51 Da), TP6 (879.83 Da), and TP8 (512.13 Da), and by complete dechlorination of the remaining products, except for TP7 (305.36 Da). The latter is a chlorinated nitrate ester, and the high chlorine content in its structure may be due to reactivity with free chlorine in solution (derived by the dechlorination reactions) or, as an alternative, to original anomalies in the polymer structure [48]. PVC dechlorination has already been reported in another study, where UV light and hydroxyl radicals significantly accelerated the dechlorination and oxidation of PVC plastics in aqueous environments [47]. In addition, the dechlorination process is also supported by the release of chlorine ions, as detected by ion chromatography (Fig. 2**(a)**).

A possible dechlorination pathway (Fig. 4**(a)**) could derive from the heterolytic photocleavage of the C-Cl bond (intermediate *i−1*), followed by dehydrogenation that could lead to the products TP5 and TP6 [49]. The formation of unsaturations in the structure, formed during the dehydrochlorination process, could facilitate the oxidative addition of $HO^{\bullet}$ radicals to the double bond, leading to the formation of dechlorinated and oxidized transformation products, such as TP3, TP4, and TP6. Another possible dechlorination pathway (Fig. 4**(a)**) could be mediated by triplet-state photosensitizers ($^3P^*$). For example, it has been observed in paraffins that the presence of a triplet-state sensitizer (such as acetone) significantly enhanced the dechlorination induced by homolytic cleavage of the C-Cl bond [49,50]. In the case of PVC, it was observed that the scavenging of $HO^{\bullet}$ by plastic particles was accounted for by the compounds released in the solution (Fig. 1**(c)**). These compounds can also act as triplet-state photosensitizers.

Mass spectrometry analysis of the aqueous phase of the PVC suspension at time zero revealed the presence of an aromatic diketone used in polymers as an UV absorber and filter, avobenzone ($C_{20}H_{22}O_3$, 311.16 Da). The identification of this compound is consistent with the detection of C=O groups by FTIR spectroscopy (see 3.3), and avobenzone is known to be responsible for the formation of a reactive triplet state [51,52]. The presence of aromatic ketones (such as avobenzone) in solution might induce triplet-state-mediated PVC dechlorination (Fig. 4 **(a)**, intermediate *i−3*), contributing to the formation of products TP1–6, TP9, and TP10. In contrast, the chlorine-rich compound TP7 could derive from the presence in solution of $Cl^{\bullet}$ radicals, which would act as chlorinating agents, of chloride, detected by ion chromatography, and of $Cl_2^{\bullet-}$ (generated by $Cl^{\bullet} + Cl^-$) [53].

Six products were identified in the case of PE (Fig. S6, TP9–14). The products would mainly derive from nitrogen addition (organic nitrates and nitro-derivatives) and dehydrogenation reactions. It is noteworthy that TP9 (274.46 Da) and TP10 (217.35 Da) are two common TPs generated from PVC and PE [30,54,55]. TP11 (107.16 Da) is the only product that contains an imine. It could be formed by transformation of an additive containing an amine group [56], the presence of which is suggested by FTIR measurements (see 3.3).

For all the polymers used in this work, the formation of nitrogen-containing TPs in different forms were observed, such as nitrate derivatives, nitro, and nitroso products (this applies for instance to all the TPs detected from PP, see Fig. S7). These products constitute the majority of the detected TPs, likely due to the nitrate concentration used in the experiments and the good ionization efficiency under HRMS experimental conditions applied in this work [57]. The formation of these compounds can be explained by the involvement of reactive species formed upon nitrate irradiation, such as $^{\bullet}NO$, $^{\bullet}NO_2$, and $^{\bullet}NO_3$ [58]. These radicals can be photogenerated according to the absorption spectrum shown in Fig. S8 [19,58], following the reactions given in Eqs. (1–3):

$$NO_3^- + h\nu \rightarrow {}^{\bullet}NO + O_2^{\bullet-} \quad (1)$$

$$NO_3^- + h\nu + H^+ \rightarrow {}^{\bullet}NO_2 + HO^{\bullet} \quad (2)$$

$$NO_3^- + HO^{\bullet} \rightarrow {}^{\bullet}NO_3 + OH^- \quad (3)$$

The possible mechanisms for the formation of *N*-derivatives are shown in Fig. 4**(b)**. After the interaction between polymer and $HO^{\bullet}$, radical intermediates such as *i−9* could be formed that would recombine with $^{\bullet}NO$, $^{\bullet}NO_2$, and $^{\bullet}NO_3$. However, since the kinetic constant of the reaction between NO_3^- and $HO^{\bullet}$ is relatively low ($k < 1.0 \times 10^5$ L mol^{-1} s^{-1}) [58], the formation of $^{\bullet}NO_3$ can be minor. Indeed, the formation of nitrate derivatives (TP7, TP12, TP15, and TP16) could also derive from the addition of $^{\bullet}NO_2$ to intermediate *i−10*. Note that the reaction of nitrogen-containing species with polymers and/or additives accounts for several TPs but would not affect kinetic competition with Bz^-, which would involve reaction with $HO^{\bullet}$ in the presence of nitrate under irradiation [23].

Moreover, the formation of carbonyl compounds and carboxylic acids (see 3.3) could be triggered by hydrogen abstraction mediated by $HO^{\bullet}$, followed by reaction with oxygen and fragmentation (see Fig. 4**(b)**, *i*−5–8). It is noteworthy that the detected TPs are relatively massive compounds with multiple functional groups. This complexity may be due to several reactions occurring on the surface of the MPs, or to the presence of anomalies in the polymers or additives. For example, the possible presence of an amine-based additive (HALS), as highlighted in the FTIR analyses (PE, Fig. 3**(d)**), may also lead to the formation of nitrogenous transformation products or piperidine derivatives from photoinduced oxidation by $HO^{\bullet}$ [59]. Future studies, with different MS ionization conditions and eventually using derivatization methods, may allow for the identification of a larger number of TPs and for a better understanding of the degradation pathways and transformation products of the MPs.

4. Conclusions

This study suggests that the reactivity of MPs (PP, PE, and PVC) with $HO^{\bullet}$ radicals is directly related to the polymer structure and the possible presence of plastic additives. PP and PE showed significant interaction with $HO^{\bullet}$, indicating that their polymeric matrices can directly scavenge $HO^{\bullet}$ radicals. In contrast, the PVC skeleton showed low reactivity with $HO^{\bullet}$ radicals, a result of their possible scavenging by organic compounds released into the solution, such as plastic additives. The kinetic competition method using NaBz is widely employed due to its high selectivity as a probe for $HO^{\bullet}$ radicals, since the reaction occurs predominantly via aromatic hydroxylation. Thus, the kinetic constant determined by this method is primarily associated with the reactivity of the $HO^{\bullet}$ radicals present in the system. However, this does not imply that the photodegradation process of MPs is controlled exclusively by $HO^{\bullet}$. Other reactive species, such as ROS and RNS, may also mediate reactions with the MPs. Therefore, assessing the individual contribution of each reactive species requires quenching experiments with selective ROS/

RNS probes, EPR/ESR spin-trapping spectroscopy, and/or the quantification of HO• radicals. These approaches are important for validating proposed mechanisms and establishing causal links between reactive species and the physicochemical transformations observed in MPs.

FTIR analysis revealed the presence of carbonyl groups, which may result from both the MPs aging process and the presence of plastic additives such as avobenzone. The integrated use of synchronous and asynchronous 2D-COS analyses can deliver high-resolution spectroscopic evidence of the sequential evolution of functional groups during MPs photoaging, thereby providing a substantially more robust mechanistic framework for elucidating degradation pathways. Small morphological changes upon irradiation could be detected by SEM, especially in the case of PP and PE. Ions quantification confirmed the formation of LMW compounds during the photodegradation of MPs, such as carboxylic acids, with production of acetate and formate for PP MPs, and of chloride for PVC MPs. The generation of chloride ions from the photodegradation of PVC MPs and/or their additives and surface impurities is supported by LC-HRMS analysis, as the detected transformation products suggest the occurrence of dechlorination processes. Nitro, nitroso, and nitrate derivatives in the TPs indicate the involvement of photoinduced species arising from nitrate such as •NO, $^{\bullet}NO_2$, and possibly $^{\bullet}NO_3$ in the transformation reactions, although further studies are needed to better understand the related chemical transformation pathways. Moreover, the relatively high concentration values of nitrate used in the irradiation experiments might overemphasize the involvement of RNS in the investigated processes.

In summary, this work provides important kinetic and reactivity information for three widely used polymers, detailing the possible transformations that these materials may undergo in sunlit waters as they naturally suffer oxidation processes, such as attack by PPRIs and, most notably, HO•. Investigation of the environmental fate of MPs serves to support the development of predictive mathematical models, and to inspire the development of actions to contain the negative impacts of MPs dispersion in the environment.

CRediT authorship contribution statement

José Luis Fonseca: Validation, Methodology, Investigation, Formal analysis, Data curation. **Raghav Dogra:** Writing – original draft, Formal analysis, Data curation. **Monica Passananti:** Writing – review & editing, Writing – original draft, Validation, Supervision, Investigation, Funding acquisition, Formal analysis. **Francesco Calore:** Writing – original draft, Formal analysis, Data curation. **Elena Badetti:** Writing – original draft, Formal analysis, Data curation. **Antonio Marcomini:** Writing – original draft, Formal analysis, Data curation. **Geovânia C. Assis:** Writing – original draft, Formal analysis, Data curation. **Luca Carena:** Writing – review & editing, Writing – original draft, Methodology, Investigation, Formal analysis, Data curation, Conceptualization. **Teixeira Antonio C. S. C.:** Writing – review & editing, Writing – original draft, Supervision, Investigation, Funding acquisition, Formal analysis, Conceptualization. **Davide Vione:** Writing – review & editing, Writing – original draft, Supervision, Resources, Methodology, Investigation, Funding acquisition, Formal analysis, Data curation, Conceptualization. **Dantas Ádila O. S.:** Writing – review & editing, Writing – original draft, Visualization, Validation, Methodology, Investigation, Formal analysis, Data curation, Conceptualization.

Consent for publication

Not applicable.

Ethics approval and consent to participate

Not applicable.

Declaration of Competing Interest

The authors declare that they have no known competing financial interests or personal relationships that could have appeared to influence the work reported in this paper.

Acknowledgments

This study was financed in part by the Coordenação de Aperfeiçoamento de Pessoal de Nível Superior – Brasil (CAPES) – Finance Code 001. A. O. S. D. and A. C. S. C. T. thank the National Council for Scientific and Technological Development (CNPq) (grants #159051/2021–5 and #309154/2023–5, respectively) and the Coordination for the Improvement of Higher Education (grant #88887.936909/2024–00). The authors would like to thank the Brazilian Nanotechnology National Laboratory (LNNano) from the Brazilian Center for Research in Energy and Materials (CNPEM) for their support. G. C. A. thanks the São Paulo Research Foundation (FAPESP, grant #2021/11590–0 and grant #2013/07296–2). This work is part of a project that has received funding from the European Research Council (ERC) under the European Union's Horizon 2020 research and innovation program, grant agreement No 948666 – ERC−2020-StG NaPuE, from MUR Call FARE project NATtA n. R20T85832Z, and from PRIN projects 2022EW9CZN (BIOPLACE) and 20227FS42S (PHOTOPLAST).

Appendix A. Supporting information

Supplementary data associated with this article can be found in the online version at doi:10.1016/j.jece.2026.123660.

Data availability

Data will be made available on request.

References

[1] A. Bianco, M. Passananti, Atmospheric micro and nanoplastics: an enormous microscopic problem, Sustainability 12 (2020) 7327.
[2] A.K. Chaudhry, P. Sachdeva, Microplastics' origin, distribution, and rising hazard to aquatic organisms and human health: socio-economic insinuations and management solutions, Reg. Stud. Mar. Sci. 48 (2021) 102018.
[3] Q. Gan, J. Cui, B. Jin, Environmental microplastics: classification, sources, fates, and effects on plants, Chemosphere 313 (2023) 137559.
[4] A. Müller, J. Brehm, M. Völkl, V. Jérôme, C. Laforsch, R. Freitag, A. Greiner, Disentangling biological effects of primary nanoplastics from dispersion paints' additional compounds, Ecotoxicol. Environ. Saf. 242 (2022) 113877.
[5] Z. Guo, D. Kodikara, L.S. Albi, Y. Hatano, G. Chen, C. Yoshimura, J. Wang, Photodegradation of organic micropollutants in aquatic environment: importance, factors and processes, Water Res. 231 (2023) 118236.
[6] T. Islam, Y. Li, M.M. Rob, H. Cheng, Microplastic pollution in Bangladesh: research and management needs, Environ. Pollut. 308 (2022) 119697.
[7] K.L. Priya, K.R. Renjith, J.J. Cindrella, M.S. Indu, S. Reji, S. Haddout, Fate, transport and degradation pathway of microplastics in aquatic environment — A critical review, Reg. Stud. Mar. Sci. 56 (2022) 102647.
[8] R.P. Schwarzenbach. Environmental Organic Chemistry, second ed., Wiley & Sons, New Jersey, 2003.
[9] D. Vione, A. Scozzaro, Photochemistry of surface fresh waters in the framework of climate change, Environ. Sci. Technol. 53 (2019) 7945–7963.
[10] B. Wu, C. Zhou, G. Zhao, J. Wang, H. Dai, T. Liu, X. Zheng, B. Chen, C. Chu, Enhanced photochemical production of reactive intermediates at the wetland soil-water interface, Water Res. 223 (2022) 118971.
[11] M. Passananti, F. Temussi, M.R. Iesce, L. Previtera, G. Mailhot, D. Vione, M. Brigante, Photoenhanced transformation of nicotine in aquatic environments: involvement of naturally occurring radical sources, Water Res. 55 (2014) 106–114.
[12] D. Vione, A test of the potentialities of the APEX software (Aqueous Photochemistry of Environmentally occurring Xenobiotics). Modelling the photochemical persistence of the herbicide cycloxydim in surface waters, based on literature kinetic data, Chemosphere 99 (2014) 272–275.
[13] H. Wiesinger, Z. Wang, S. Hellweg, Deep dive into plastic monomers, additives, and processing aids, Environ. Sci. Technol. 55 (2021) 9339–9351.
[14] J. Duan, Y. Li, J. Gao, R. Cao, E. Shang, W. Zhang, ROS-mediated photoaging pathways of nano- and micro-plastic particles under UV irradiation, Water Res. 216 (2022) 118320.
[15] J.N. Hahladakis, C.A. Velis, R. Weber, E. Iacovidou, P. Purnell, An overview of chemical additives present in plastics: migration, release, fate and environmental

impact during their use, disposal and recycling, J. Hazard. Mater. 344 (2018) 179–199.
[16] D. Fabbri, L. Carena, D. Bertone, M. Brigante, M. Passananti, D. Vione, Assessing the photodegradation potential of compounds derived from the photoinduced weathering of polystyrene in water, Sci. Total. Environ. 876 (2023) 162729.
[17] A. Bianco, F. Sordello, M. Ehn, D. Vione, M. Passananti, Degradation of nanoplastics in the environment: reactivity and impact on atmospheric and surface waters, Sci. Total. Environ. 742 (2020) 140413.
[18] X. Zhou, K. Mopper, Determination of photochemically produced hydroxyl radicals in seawater and freshwater, Mar. Chem. 30 (1990) 71–88.
[19] G.V. Buxton, C.L. Greenstock, W.P. Helman, A.B. Ross, Critical review of rate constants for reactions of hydrated electrons, hydrogen atoms and hydroxyl radicals (•OH/•O−) in aqueous solution, J. Phys. Chem. Ref. Data 17 (1988) 513–886.
[20] Y. Qiu, T. Zhang, P. Zhang, Fate and environmental behaviors of microplastics through the lens of free radical, J. Hazard. Mater. 453 (2023) 131401.
[21] J.M. Allen, S.K. Allen, S.W. Baertschi, 2-Nitrobenzaldehyde: a convenient UV-A and UV-B chemical actinometer for drug photostability testing, J. Pharm. Biomed. Anal. 24 (2000) 167–178.
[22] H.S. Fogler. Elements of Chemical Reaction Engineering, 4th ed., Pearson, New Jersey, 2009.
[23] J.J. Jankowski, D.J. Kieber, K. Mopper, Nitrate and nitrite ultraviolet actinometers, Photochem. Photobiol. 70 (1999) 319–328.
[24] A. Jansson, K. Möller, T. Gevert, Degradation of post-consumer polypropylene materials exposed to simulated recycling—mechanical properties, Polym. Degrad. Stab. 82 (2003) 37–46.
[25] K. Zhao, Z. Zhang, Y. Li, H. Fu, X. Peng, R. Tao, Z. Zhang, Y. Li, H. Fu, X. Peng, R. Tao, Identifying the flows and stocks of additives in polyvinyl chloride plastics for balancing environmental and economic impacts, Resour. Conserv. Recycl. 217 (2025) 108213.
[26] R. Yang, H. Cao, H. Dong, X. Wang, The mechanism of UV accelerated aging of polyvinyl chloride in marine environment: the role of free radicals, Mar. Pollut. Bull. 207 (2024) 116736.
[27] K. Zhu, H. Jia, Y. Sun, Y. Dai, C. Zhang, X. Guo, T. Wang, L. Zhu, Long-term phototransformation of microplastics under simulated sunlight irradiation in aquatic environments: roles of reactive oxygen species, Water Res. 173 (2020) 115564.
[28] L. He, W. Zhuang, J. Hur, L. Yang, Interactions of microplastics, dissolved organic matter, and coexisting pollutants: mechanisms, environmental implications, and knowledge gaps, Environ. Res. 289 (2026) 123418.
[29] R. Darvishi, M.N. Esfahany, R. Bagheri, S-PVC grain morphology: a review, Ind. Eng. Chem. Res. 54 (2015) 10953–10963.
[30] B. Gewert, M. Plassmann, O. Sandblom, M. Macleod, Identification of chain scission products released to water by plastic exposed to ultraviolet light, Environ. Sci. Technol. Lett. 5 (2018) 272–276.
[31] P. Lestari, Y. Trihadiningrum, I. Warmadewanthi, Simulated degradation of low-density polyethylene and polypropylene due to ultraviolet radiation and water velocity in the aquatic environment, J. Environ. Chem. Eng. 10 (2022) 107553.
[32] Z. Ouyang, Z. Zhang, Y. Jing, L. Bai, M. Zhao, X. Hao, X. Li, X. Guo, The photo-aging of polyvinyl chloride microplastics under different UV irradiations, Gondwana Res. 108 (2022) 72–80.
[33] B.C. Smith, The Infrared Spectra of Polymers III: hydrocarbon polymers, Spectroscopy 36 (2021) 22–25.
[34] J. Fang, L. Zhang, D. Sutton, X. Wang, T. Lin, Needleless melt-electrospinning of polypropylene nanofibres, J. Nanomater. 2012 (2012) 1–9.
[35] M.D. Green, F.J. Guild, R.D. Adams, Characterisation and comparison of industrially pre-treated homopolymer polypropylene, HF 135M, Int. J. Adhes. Adhes. 22 (2002) 81–90.
[36] M. Namie, J. Kim, S. Yonezawa, Improving the Dyeing of Polypropylene by Surface Fluorination, Colorants 1 (2022) 121–131.
[37] J.V. Gulmine, P.R. Janissek, H.M. Heise, L. Akcelrud, Polyethylene characterization by FTIR, Polym. Test. 21 (2002) 557–563.
[38] R.L. Kovács, M. Csontos, S. Gyöngyösi, J. Elek, B. Parditka, G. Deák, Á. Kuki, S. Kéki, Z. Erdélyi, Surface characterization of plasma-modified low density polyethylene by attenuated total reflectance fourier-transform infrared (ATR-FTIR) spectroscopy combined with chemometrics, Polym. Test. 96 (2021) 107080.
[39] R. Okubo, A. Yamamoto, A. Kurima, T. Sakabe, Y. Ide, A. Isobe, Estimation of the age of polyethylene microplastics collected from oceans: application to the western north Pacific Ocean, Mar. Pollut. Bull. 192 (2023) 114951.
[40] Thermo Fisher Scientific. (2004). Fundamentals of polymer analysis. ⟨http://tools.thermofisher.com/content/sfs/brochures/Fundamentals-Polymer-Analysis.pdf⟩.
[41] T. Andjelković, D. Bogdanović, I. Kostić, G. Kocić, G. Nikolić, R. Pavlović, Phthalates leaching from plastic food and pharmaceutical contact materials by FTIR and GC-MS, Environ. Sci. Pollut. Res. 28 (2021) 31380–31390.
[42] R. Bodîrlău, C.A. Teacă, I. Spiridon, Preparation and characterization of composites comprising modified hardwood and wood polymers/poly(vinyl chloride), BioResour 4 (2009) 1285–1304.
[43] P.P.R. Cruz, L.C. Silva, R.A. Fiuza-Jr, H. Polli, Thermal dehydrochlorination of pure PVC polymer: Part I—thermal degradation kinetics by thermogravimetric analysis, J. Appl. Polym. Sci. 138 (2021) e50598.
[44] S. Klempová, M. Oravec, K. Vizárová, Analysis of thermally and UV–Vis aged plasticized PVC using UV–Vis, ATR-FTIR and Raman spectroscopy, Spectrochim. Acta A Mol. Biomol. Spectrosc. 294 (2023) 122541.
[45] A. Klisińska-Kopacz, B. Łydšba-Kopczyńska, M. Czarnecka, T. Koűlecki, J. H. Mélendez, A. Mendys, A. Kłosowska-Klechowska, M. Obarzanowski, P. Frączek, Raman spectroscopy as a powerful technique for the identification of polymers used in cast sculptures from museum collections, J. Raman Spectrosc. 50 (2018) 213–221.
[46] E.L. Schymanski, J. Jeon, R. Gulde, K. Fenner, M. Ruff, H.P. Singer, J. Hollender, Identifying Small Molecules via High Resolution Mass Spectrometry: Communicating Confidence, Environ. Sci. Technol. 48 (2014) 2097–2098.
[47] C. Wang, Z. Xian, X. Jin, S. Liang, Z. Chen, B. Pan, B. Wu, Y.S. Ok, C. Gu, Photo-aging of polyvinyl chloride microplastic in the presence of natural organic acids, Water Res. 183 (2020) 116082.
[48] K. Endo, N. Kaneda, H. Waku, M. Saitoh, N. Emori, Synthesis and structure of poly (vinyl chloride), Prog. Polym. Sci. 27 (2002) 2021–2054.
[49] W. Zhang, Y. Gao, Y. Qin, M. Wang, J. Wu, G. Li, T. An, Photochemical degradation kinetics and mechanism of short-chain chlorinated paraffins in aqueous solution: A case of 1-chlorodecane, Environ. Pollut. 247 (2019) 362–370.
[50] I. Koh, W. Thiemann, Study of photochemical oxidation of standard chlorinated paraffins and identification of degradation products, J. Photochem. Photobiol. A Chem. 139 (2001) 205–215.
[51] J.A. Berenbeim, N.G.K. Wong, M.C.R. Cockett, G. Berden, J. Oomens, A.M. Rijs, C. E.H. Dessent, Unravelling the keto–enol tautomer dependent photochemistry and degradation pathways of the protonated UVA filter avobenzone, J. Phys. Chem. A. 124 (2020) 2919–2930.
[52] V. Marturano, P. Cerruti, V. Ambrogi, Polymer additives, Phys. Sci. Rev. 2 (2017) 1–20.
[53] P. Neta, R.E. Huie, A.B. Ross, Rate constants for reactions of inorganic radicals in aqueous solution, J. Phys. Chem. Ref. Data 17 (1988) 1027–1284.
[54] M. Passananti, F. Temussi, M.R. Iesce, G. Mailhot, M. Brigante, The impact of the hydroxyl radical photochemical sources on the rivastigmine drug transformation in mimic and natural waters, Water Res. 47 (2013) 5422–5430.
[55] S. Rossignol, L. Tinel, A. Bianco, M. Passananti, M. Brigante, D.J. Donaldson, C. George, Atmospheric photochemistry at a fatty acid-coated air-water interface, Science 353 (2016) 699–702.
[56] X. Wu, Z. Tan, R. Liu, Z. Liao, H. Ou, Gaseous products generated from polyethylene and polyethylene terephthalate during ultraviolet irradiation: Mechanism, pathway and toxicological analyses, Sci. Total. Environ. 876 (2023) 162717.
[57] A. Hilkert, J.K. Böhlke, S.J. Mroczkowski, K.L. Fort, K. Aizikov, X.T. Wang, S. H. Kopf, C. Neubauer, Exploring the potential of electrospray-orbitrap for stable isotope analysis using nitrate as a model, Anal. Chem. 93 (2021) 9139–9148.
[58] J. Mack, J.R. Bolton, Photochemistry of nitrite and nitrate in aqueous solution: A review, J. Photochem. Photobiol. A Chem. 128 (1999) 1–13.
[59] G. Gryn'ova, K.U. Ingold, M.L. Coote, New insights into the mechanism of amine/nitroxide cycling during the hindered amine light stabilizer inhibited oxidative degradation of polymers, J. Am. Chem. Soc. 134 (2012) 12979–12988.